Shape-based multi-region segmentation framework: application to 3D infants MRI data

Sonia Dahdouh [a] and Isabelle Bloch [a]

[a]Institut Mines-Telecom, Telecom ParisTech, CNRS-LTCI, 46 rue Barrault, 75013, Paris

ABSTRACT

This paper presents a novel shape-guided multi-region variational region growing framework for extracting simultaneously thoracic and abdominal organs on 3D infants whole body MRI. Due to the inherent low quality of these data, classical segmentation methods tend to fail at the multi-segmentation task. To compensate for the low resolution and the lack of contrast and to enable the simultaneous segmentation of multiple organs, we introduce a segmentation framework on a graph of supervoxels that combines supervoxels intensity distribution weighted by gradient vector flow value and a shape prior per tissue. The intensity-based homogeneity criteria and the shape prior, encoded using Legendre moments, are added as energy terms in the functional to be optimized. The intensity-based energy is computed using both local (voxel value) and global (neighboring regions mean values, adjacent voxels values and distance to the neighboring regions) criteria. Inter-region conflict resolution is handled using a weighted Voronoi decomposition method, the weights being determined using tissues densities. The energy terms of the global energy equation are weighted using an information on growth direction and on gradient vector flow value. This allows us to either guide the segmentation toward the image natural edges if it is consistent with image and shape prior terms, or enforce the shape prior term otherwise. Results on 3D infants MRI data are presented and compared to a set of manual segmentations. Both visual comparison and quantitative measurements show good results.

1. INTRODUCTION

In order to assess the impact of radiofrequency waves on the human body, numerical dosimetry studies on whole body 3D models are performed. One of the most reliable way to build these 3D models is by constructing voxelized models based on 3D medical data segmentations which raises the need to develop dedicated multi-organs segmentation methods.

The problem of the simultaneous segmentation of multiple abdominal organs is a challenge, addressed only recently. In Wolz *et al.*,[1] the authors used a hierarchical atlas registration method for generating subject-specific priors, and graph-cuts are used to obtain the final segmentation of the liver, kidneys, pancreas and spleen. Probabilistic atlases were used as a prior knowledge by Park *et al.*[2] and Shimizu *et al.*,[3] while statistical models were used by Okada *et al.*[4] Linguraru *et al.*[5] combined statistical atlases with a 4D directional graph to segment the liver, the spleen and both kidneys. Random forests were used for organs localization on adults CT Liver data by Gauriau *et al.*[6] and was further extended to multi-organs localization in.[7] However, the methods developed so far for abdominal multi-organs segmentation are concentrated almost exclusively on CT data which are scarce and hard to obtain when dealing wih newborn and infants.

While still difficult to obtain, 3D MRI images are more and more available. They however suffer from strong artifacts such as low resolution and contrast, high noise, strong anisotropy, partial volume effect and blurring effects due to the child movements.

Corresponding author e-mail: sonia.dahdouh@gmail.com

Medical Imaging 2015: Image Processing, edited by Sébastien Ourselin, Martin A. Styner, Proc. of SPIE Vol. 9413, 941312 · © 2015 SPIE · CCC code: 1605-7422/15/$18 · doi: 10.1117/12.2082038

The aim of this paper is thus to develop a multi-organ segmentation method for newborn and infant whole body 3D MRI data. We propose here to integrate multiple shape constraints into a new 3D multi-region variational region growing (VRG) framework, extending the mono-region VRG described by Rose *et al.*[8] and Revol-Muller *et al.*,[9] and taking advantage of a shape prior encoded with Legendre moments as done in Dahdouh *et al.*[10] or Foulonneau *et al.*[11] Global and local information is used in the proposed intensity-based energy. Regions conflict resolution is handled with a weighted Voronoi based approach using tissues density as a prior. Results on 3D newborn MRI are presented in Section 3.

2. METHOD

With the aim of segmenting simultaneously multiple tissues, the idea to extend VRG[8] into a multi-region framework with multiple shape priors has emerged. However, due to the difficulty for classical region growing methods to deal with noisy data, a straightforward extension of the VRG method to a multi-region one was not efficient and we thus propose a multi-region algorithm, as detailed next.

2.1 Supervoxel graph construction

To deal with the high level of noise in our data as well as the partial volume effects, the 3D volume is first decomposed in a set of supervoxels using the SLIC algorithm.[12] The method proposed by Achanta *et al.*[12] uses a k-means clustering to generate superpixels, where distances from a cluster center to pixels are only computed in a pre-defined vicinity.

In the remainder of the algorithm, all steps will be applied on the adjacency graph of supervoxels, each node v being characterized by the supervoxel center spatial position, the average grey level value of the voxels it contains and its adjacent nodes.

It has to be noted that although this information reduction step could make difficult the segmentation of really small structures, the resolution of the MRI data we are dealing with does not allow the imaging of such tissues. Thus, the proposed reduction step does not hamper the performances of the thereafter presented method.

2.2 Shape guided multi-region variational region growing

The core of the method proposed here is the simultaneous evolution of a set of N regions to find the optimal partition of the image in a set of $N+1$ regions, the $(N+1)$th one being the background.

Let Ω be a bounded and open subset of $\mathbf{R}^3$ and $\mathrm{I} : \Omega \to \mathbf{R}$ an image.
Ω_{in}^i represents the segmented region i and is a subset of Ω, Φ_i represents the characteristic function of the evolving region i and Φ_i^n, the characteristic function at iteration n.

The characteristic function is thus defined as:

$$\begin{aligned} \Phi_i \quad : \quad & \Omega \to \{0,1\} \\ & x \longmapsto \begin{cases} 1, & \text{if } x \in \Omega_{in}^i \\ 0, & \text{otherwise} \end{cases} \end{aligned}$$

We first consider that, within the minimization procedure, a node can have different labels at a same time and can thus belong to different regions simultaneously. However, from a region point of view, a node can only have two different states: belonging to the inside region or not.

The label modification of a given candidate node v at iteration $n+1$ can thus be expressed as:

$$\Phi_i^{n+1}(v) = 1 - \Phi_i^n(v) \tag{1}$$

and $\Phi_i^{n+1}(x) = \Phi_i^n(x)$ if $x \neq v$ and $x \in \Omega$.

2.2.1 Image-based energy

Using the previously defined notions, we can then define the image-based energy as:

$$E_{image} = \sum_{i=1}^{N} J_{image}(\Omega_{in}^i) \qquad (2) \qquad \text{with} \quad J_{image}(\Omega_{in}^i) = \int_{\Omega_{in}^i} k_x dx \qquad (3)$$

k_x being approximated as a region-independent descriptor. As in Revol-Muller *et al.*,[9] we replace Ω_{in}^i by the associated characteristic function $\Phi_i^n(x)$ defined on Ω and the previous equation can thus be rewritten in the discrete case as:

$$J(\Phi_i^n(x)) = \sum_{x \in \Omega} k_x . \Phi_i^n(x) \qquad (4)$$

While the classical Chan and Vese[13] energy has been used in[8] or,[9] the low quality of data has led us to develop a new image-based energy taking into account information on all the evolving regions at the same time as well as information on adjacent nodes memberships. This energy can be defined as:

$$\begin{aligned} J_{image}(\Phi_i^n) \quad = \quad & \sum_{x \in \Omega} [|I(x) - \mu_i|^2 + \frac{1}{N_{aj_x}} \sum_{y \in aj_x} |I(y) - \mu_i|^2] . \Phi_i^n(x) \\ & + \sum_{x \in \Omega} [\sum_{r \neq i} \lambda(x,r) |I(x) - \mu_r|^2 + \frac{1}{2N_{aj_x}} \sum_{y \in aj_x} \sum_{r \neq i} \lambda(y,r) |I(y) - \mu_r|^2] . (1 - \Phi_i^n(x)) \end{aligned}$$

with μ_i the mean gray level value of region i, computed at each iteration, and aj_x the set of adjacent nodes to x, of cardinality N_{aj_x}.

Finally, $\lambda(x,r)$ is a weighting function to take into account the spatial proximity of all the other regions into the image, including the background:

$$\lambda(x,r) = \frac{\sum_{p \in \{1..N\}} d(x, \Omega_{in}^p) - d(x, \Omega_{in}^r)}{(N-1) \sum_{p \in \{1..N\}} d(x, \Omega_{in}^p)} \qquad (5)$$

with $d(x, \Omega_{in}^r))$ the minimal Euclidean distance between a node x and all the nodes of a given region p.

Results of the segmentation procedure using this energy into a multi-region VRG with no shape prior are illustrated in Figure 1 (b) and (c) (Only one slice is displayed, but the whole process is applied in 3D). The use of this energy is compared to the classical Chan and Vese[13] one. As we can see, the new energy allows a more accurate segmentation of the different structures. However, when dealing with such noisy data, it is not sufficent to achieve an accurate segmentation of the different organs.

An additional information based on a shape prior on each tissue is thus added, as described next.

2.2.2 Shape constraint

In order to constraint the evolving regions toward the final correct shape of the considered organ, a shape prior per-region is used. While numerous methods have been proposed to constrain shape in a level-set based segmentation energy functional[10,11,14] , few authors have dealt with the problem of the introduction of a shape prior in a region growing framework. In Rose *et al.*[8] , Tchebichef moments are used and made invariant to affine transformation using the 2D method described by Pey *et al.*[15]

Following the work of Foulonneau *et al.*,[11] we decided here to use Legendre moments, and the method proposed in this paper optimizes, within a multi-region VRG segmentation framework, a prior model per region represented by the distance computed between the currently determined shape, represented by its Legendre moments and a set of Legendre moments computed on the registered prior shape.

(a) (b) (c) (d)

Figure 1. Segmentation of brain, lungs, liver and kidneys for a 2 years old child. (a) One slice of the original MRI volume. (b) Segmentation results with the Chan and Vese[13] energy, no shape prior and no conflicts resolution. (c) With the proposed energy, no shape prior and no conflicts resolution. (d) With the proposed energy, shape priors and conflicts resolution scheme.

Shape encoding with Legendre moments.

Let $I : [-1, 1]^3 \rightarrow \mathbf{R}$ be a 3D binary image encoding a shape where spatial coordinates are normalized in $[-1, 1]$.

The $(p + q + r)^{th}$ order 3D Legendre moments of the image are defined as:

$$L_{pqr} = \lambda_{pqr} \int_{[-1,1]^3} P_p(x) P_q(y) P_r(z) I(x, y, z) \mathrm{d}x\mathrm{d}y\mathrm{d}z \tag{6}$$

with $\lambda_{pqr} = \frac{(2p+1)(2q+1)(2r+1)}{8}$, $(p, q, r) \in \mathbf{N^3}$ and P_i $(i = p, q, r)$, the Legendre polynomial defined as:

$$P_i(x) = \sum_{k=0, i-k=even}^{i} (-1)^{\frac{i-k}{2}} \frac{1}{2^i} \frac{(i + k)! x^k}{(\frac{i-k}{2})!(\frac{i+k}{2})!k!} \tag{7}$$

With η, a finite number of moments for each dimension, an estimate of I can be given by:

$$\widetilde{I}(x, y, z) = \sum_{p=0}^{\eta} \sum_{q=0}^{p} \sum_{r=0}^{q} \lambda_{p-q,q-r,r} P_{p-q}(x) P_{q-r}(y) P_r(z) \tag{8}$$

The computation of the 3D Legendre moments are performed using the fast method proposed by Hosny.[16] Since 3D Legendre moments are not invariant to affine transformations, a prior registration step is needed before performing the moments decomposition. The shape prior and the growing region are thus meshed and then registered using a registration method based on the one proposed by Guy *et al.*[17] A global transformation is first estimated using a principal component analysis decomposition on the normal field of the mesh. An Iterative Closest Point[18] algorithm is then used to perform local adjustments to optimize the registration process. The registered prior is then rasterized and the Legendre moments are computed.

Introducing a shape constraint into the multi-region VRG framework.
An L_2 distance is defined in order to compare the shape of the evolving region i with the corresponding reference shape ref. The shape prior energy is thus defined as:

$$J_{prior}(\Phi_i^n) = \sum_{p,q,r}^{p,q,r<\eta} H_{pqr}(\sigma)^2.(L_{pqr}(\Omega_{in}^i)) - L_{pqr}^{ref})^2 \tag{9}$$

with η the maximal Legendre moment order, σ a hyper-parameter and

$$H_{pqr}(\sigma) = \frac{1}{\sqrt{2\pi\sigma^2}} \exp^{-\frac{(p+q+r)^2}{2\sigma^2}} \tag{10}$$

the weighting matrix proposed by Revol-Muller *et al.*[9]

2.2.3 Global energy

The segmentation depending on both gray-level intensity values and the shape prior of each region in the image, the variation of the global energy, defined as the weighted sum of all the above presented energies, is formulated as:

$$\Delta J(\Phi_i^n(v)) = (1 + \tau(v))\Delta J_{image} + \beta(1 - \tau(v))\Delta J_{prior} \tag{11}$$

with β a hyper-parameter balancing the respective influences of the shape and intensity priors.

$\tau(v)$ is a weighting term used to guide the segmentation process toward image natural edges. It is defined as the scalar product of the normalized growing direction at a node v and the normalized gradient vector flow value at this same node.

2.2.4 Inter-region conflict resolution

As we have seen previously, the energy minimization procedure considers that a node can belong simultaneously to different regions. Since we want to obtain separate segmented regions in the final segmentation procedure, an inter-region conflict resolution scheme has been added whenever a conflict appears.
A conflict between two regions arises when a node is claimed by more than one region. When a conflict arises, the conflictual node cv as well as all the following conflictual nodes agglomerated in the following iterations as a consequence of the agglomeration of cv are marked as conflictual. The region boundaries rb before the addition of cv are saved. All the conflictual nodes claimed by the same set of regions are agglomerated in a virtual region vr as shown in Figure 2. The number of virtual regions is equal to the number of conflicts between sets of regions. When a virtual region vr stops growing, i.e. when its energy stops decreasing, a Voronoi based decomposition procedure is applied to vr whose seeds are the nodes of rb that led to the addition of the conflictual nodes as shown in Figure 3.

Starting from the boundaries rb of all the regions involved in a conflict, a Voronoi spatial decomposition algorithm is propagated for each region using a different speed factor for each region. The final Voronoi decomposition between all candidate regions determine the cv voxels final region membership.

2.2.5 Parameterization

Number of Legendre moments. Since we want the shape prior to guide the segmentation toward a shape looking alike the shape prior but we also want to be able to capture anatomical variations, the number of Legendre has been set to 30 for all the experiments performed in this paper. This number has been found as a good tradeoff between global shape capture and computational time.

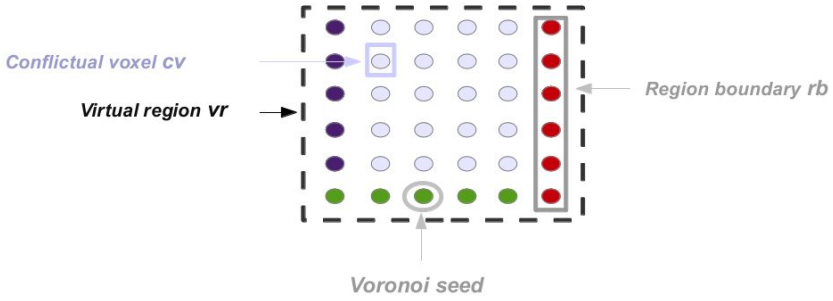

Figure 2. Conflictual region composition.

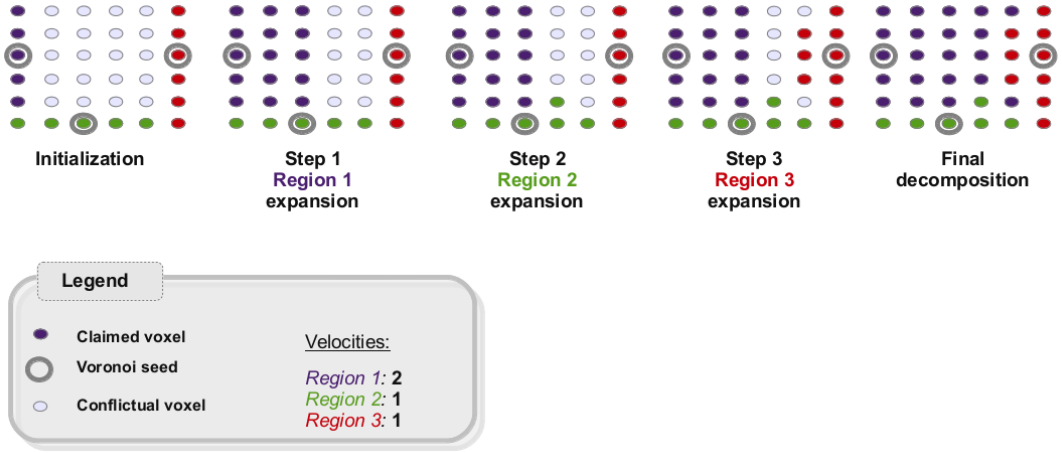

Figure 3. Voronoi decomposition of a conflictual region using different regions velocities.

Seeds determination. In order to initiate the segmentation procedure, seeds have to be given for each organ. A single point (which would correspond to a supervoxel structure) or a small region given by the user is usually enough to obtain reliable results. For complicated structures, a rough skeleton of the organ on one slice of the 3D volume can be given to improve the segmentation results.

Voronoi decomposition speed factor. The speed factor used here represents the hardness of a material, i.e. its inherent capacity to be deformed under the pressure of neighboring structures, and is a hyper-parameter given by the user. For medical images, a good speed factor can be obtained using the magnitude ratio between organs density values. The magnitude ratio between young modulus could also be used. Indeed, higher is the density, less deformable the organ is. It translates here by the fact that if the segmentation procedure detects that a voxel could belong either to a bony structure or a soft tissues one, then the probability that the soft tissue at this place is deformed when compared to the reference tissue shape prior is higher than the probability that the bony structure is deformed when compared to the reference bony shape prior. We thus consider that the priority should be given to the bony structure for the final voxel membership value.

A comparison of the segmentation results obtained with the segmentation algorithm without and with the shape constraint is shown in Figure 1(c) and (d). As seen in these figures, using the shape priors improves greatly the organs segmentation.

3. RESULTS AND DISCUSSION

In order to assess the performances of the proposed method, six whole body 3D MRI data (T1 and T2 sequences) of infants from 5 months to 3 years and 1 months old have been segmented and compared with manual segmentations performed by an expert. The tissues of the 5 years old child model from the Virtual Family[19] have been used as shape priors. Seven structures have been segmented: both left and right lungs, the liver, both kidneys, the spleen and the brain (considered as a unique tissue and composed of both white and grey matter). For each volume, a visual validation of the segmentation result was performed as illustrated in Figure 1 (d). Manual segmentations being available for 5 of the volumes, a comparison between manual and automatic segmentations has thus been carried out. Dice, sensitivity and specificity mean values per tissue for all volumes are reported in Table 1.

Table 1. Quantitative results. Dice, sensitivity and specificity indices computed between automatic and manual segmentations of the different tissues.

Tissue	Dice index	Sensitivity index	Specificity index
Both lungs	0.85	0.9	0.99
Both kidneys	0.7	0.71	0.99
Liver	0.86	0.93	0.99
Spleen	0.78	0.8	0.99
Brain	0.89	0.82	0.99

As we can see, the proposed segmentation framework allows a good simultaneous segmentation of several abdominal and thoracic structures as well as brain on low quality data. The lower sensitivity index compared to specificity one shows a tendancy of the method to slighty underestimate the structures size. This comes mainly from two points: the use of supervoxels in the segmentation scheme and the smoothing performed by the use of adjacent supervoxels intensities in the image-based energy who tends to have a blurring effect on actual contours positions. On data with a higher quality, we could imagine to use directly voxels data and thus to limit this effect or add a post-processing step who would split regions boundary supervoxels and then reapply the segmentation process on these voxels.

4. CONCLUSION

In order to segment simultaneously multiple organs on 3D MRI whole body volumes, a shape-guided multi-regions VRG segmentation framework has been presented in this paper. This 3D segmentation methods embeds local and global intensity criteria computation on the supervoxel graph and a shape prior per tissue. Shape information is encoded with Legendre moments and a new image-based energy has been presented. Inter-region conflict is handled using a Voronoi based method combining Voronoi space decomposition and organs density priors. The initialization of the segmentation process is performed semi-automatically by asking the user to determine a seed inside each considered organ. Tests on clinical cases provided good results when compared visually and quantitatively with manual segmentation. To evaluate the genericity of our method, it has also been applied successfully on adults abdominal CT data. A straightforward improvement of the method would be the automatic determination of seeds. A more complex improvement would be to deal with topological changes. Indeed, while one of the main advantages of region growing methods is the ability to handle topological changes, the addition of a shape prior strongly reduces this ability thus limiting the extension of the approach to structures such as whole skeleton or arterial structures, except if the topology is also encoded in the shape prior.

ACKNOWLEDGMENTS

This work has been supported by a grant from ANSES within the ACTE project. The authors would like to thank Dr. Alison from Robert Debré Hospital and Dr. Morel from Trousseau Hospital for the data. We also would like to thank Dr. Memari and E. Guy for the fruitfull discussions on Voronoi segmentation and meshes registration. We would also like to thank Joe Wiart and his team at Orange Labs for their collaboration.

REFERENCES

[1] Wolz, R., Chu, C., Misawa, K., Fujiwara, M., Mori, K., and Rueckert, D., "Automated abdominal multi-organ segmentation with subject-specific atlas generation," *IEEE Transactions on Medical Imaging* **32**(9), 1723–1730 (2013).

[2] Park, H., Bland, P., and Meyer, C., "Construction of an abdominal probabilistic atlas and its application in segmentation," *IEEE Transactions on Medical Imaging* **22**(4), 483–492 (2003).

[3] Shimizu, A., Ohno, R., Ikegami, T., Kobatake, H., Nawano, S., and Smutek, D., "Segmentation of multiple organs in non-contrast 3D abdominal CT images," *International Journal of Computer Assisted Radiology and Surgery* **2**(3-4), 135–142 (2007).

[4] Okada, T., Yokota, K., Hori, M., Nakamoto, M., Nakamura, H., and Sato, Y., "Construction of hierarchical multi-organ statistical atlases and their application to multi-organ segmentation from CT images," in [*Medical Image Computing and Computer-Assisted Intervention, MICCAI 2008, LNCS*], **5241**, 502–509 (2008).

[5] Linguraru, M. G., Pura, J. A., Pamulapati, V., and Summers, R. M., "Statistical 4D graphs for multi-organ abdominal segmentation from multiphase CT," *Medical Image Analysis* **16**(4), 904–914 (2012).

[6] Gauriau, R., Cuingnet, R., Prevost, R., Mory, B., Ardon, R., Lesage, D., and Bloch, I., "A generic, robust and fully-automatic workflow for 3D CT liver segmentation," in [*Abdominal Imaging. Computation and Clinical Applications - 5th International Workshop, Held in Conjunction with MICCAI 2013, Nagoya, Japan, September 22, 2013. Proceedings*], 241–250 (2013).

[7] Gauriau, R., Cuingnet, R., Lesage, D., and Bloch, I., "Multi-organ localization combining global-to-local regression and confidence maps," in [*Medical Image Computing and Computer-Assisted Intervention - MICCAI 2014 - 17th International Conference, Boston, MA, USA, September 14-18, 2014, Proceedings, Part III*], 337–344 (2014).

[8] Rose, J., Revol-Muller, C., Reichert, C., and Odet, C., "Variational region growing," in [*VISAPP-09 International Conference on Computer Vision Theory and Applications*], (2009).

[9] Revol-Muller, C., Rose, J., Pacureanu, A., Peyrin, F., and Odet, C., "Shape prior in variational region growing," in [*3rd International Conference on Image Processing Theory, Tools and Applications (IPTA)*], 116–120 (2012).

[10] Dahdouh, S., Serrurier, A., Grangé, G., Angelini, E., and Bloch, I., "Segmentation of fetal envelope from 3D ultrasound images based on pixel intensity statistical distribution and shape priors," in [*International Symposium on Biomedical Imaging: From Nano to Macro ISBI'13*], 1014–1017 (2013).

[11] Foulonneau, A., Charbonnier, P., and Heitz, F., "Multi-reference shape priors for active contours," *International Journal of Computer Vision* **81**(1), 68–81 (2009).

[12] Achanta, R., Shaji, A., Smith, K., Lucchi, A., Fua, P., and Su, S., "SLIC superpixels compared to state-of-the-art superpixel methods," *IEEE Transactions on Pattern Analysis and Machine Intelligence* **34**(11), 2274–2282 (2012).

[13] Chan, T. F. and Vese, L. A., "Active contours without edges," *IEEE Transactions on Image Processing* **10**(2), 266–277 (2001).

[14] Wojak, J., Angelini, E. D., and Bloch, I., "Introducing shape constraint via Legendre moments in a variational framework for cardiac segmentation on non-contrast CT images.," in [*VISAPP, International Conference on Computer Vision Theory and Applications*], 209–214 (2010).

[15] Pei, S.-C. and Lin, C.-N., "Image normalization for pattern recognition," *Image and Vision Computing* **13**(10), 711 – 723 (1995).

[16] Hosny, K. M., "Fast and low-complexity method for exact computation of 3D Legendre moments," *Pattern Recognition Letters* **32**(9), 1305–1314 (2011).

[17] Guy, E., Thiery, J.-M., and Boubekeur, T., "Simselect: Similarity-based selection for 3D surfaces," *Computer Graphics Forum* **33**(2), 165–173 (2014).

[18] Besl, P. J. and Mckay, H. D., "A method for registration of 3-D shapes," *IEEE Transactions on Pattern Analysis and Machine Intelligence* **14**(2), 239–256 (1992).

[19] Gosselin, M.-C., Neufeld, E., Moser, H., Huber, E., Farcito, S., Gerber, L., Jedensj, M., Hilber, I., Gennaro, F. D., Lloyd, B., Cherubini, E., Szczerba, D., Kainz, W., and Kuster, N., "Development of a new generation of high-resolution anatomical models for medical device evaluation: the virtual population 3.0," *Physics in Medicine and Biology* **59**(18), 5287 (2014).